Hindawi Publishing Corporation
Advances in Condensed Matter Physics
Volume 2015, Article ID 736517, 7 pages
http://dx.doi.org/10.1155/2015/736517

Research Article

Analysis of Eu^{3+} Emission from Mg_2TiO_4 Nanoparticles by Judd-Ofelt Theory

Katarina Vuković, Mina Medić, Milica Sekulić, and Miroslav D. Dramićanin

Vinča Institute of Nuclear Sciences, University of Belgrade, P.O. Box 522, 11000 Belgrade, Serbia

Correspondence should be addressed to Miroslav D. Dramićanin; dramican@vinca.rs

Received 5 May 2015; Revised 30 June 2015; Accepted 5 July 2015

Academic Editor: Mohindar S. Seehra

Eu^{3+} doped Mg_2TiO_4 (2 at% of Eu) nanoparticles which are 5 to 10 nm in diameter are prepared by Pechini-type polymerized complex route followed with the calcination in the temperature range from 400°C to 700°C. Emission spectra display characteristic $^5D_0 \rightarrow {}^7F_J$ ($J = 0, 1, 2, 3$, and 4) spin forbidden f-f electronic transitions of the Eu^{3+} ions with the most pronounced emission coming from $^5D_0 \rightarrow {}^7F_2$ transition and with the emission decays varying between 0.57 and 0.87 ms for samples prepared at different temperatures. Judd-Ofelt theoretical analysis of the emission spectra of Eu^{3+} ions was performed, which allowed calculating radiative and nonradiative emission probabilities, Judd-Ofelt intensity parameters, and the quantum efficiency of the Eu^{3+} emission in the Mg_2TiO_4 nanoparticles. The analyses showed the existence of high asymmetry around the metal ion sites. Also, the largest quantum efficiency of emission of 58.5% is found in nanoparticles prepared at 600°C.

1. Introduction

Magnesium-orthotitanate (Mg_2TiO_4) is a dielectric for microwave technology, a heat resistor, a capacitor for temperature compensation, and a refractory material. Strong, deep-red emission can be achieved by incorporation of Mn^{4+} ions in its structure [1, 2], and the emission is used to improve the color-rendering index of phosphor-converted white-light-emitting diodes. Luminescence from Mg_2TiO_4 can be also realized with the incorporation of trivalent rare earth (RE) ions in its structure since the band gap of the material is large enough (Eg ~ 3,7 eV) to accommodate RE energy levels. Then, Mg_2TiO_4 can serve as a phosphor of different colors depending on the RE ion used as an activator. In this sense, nanoparticles of Mg_2TiO_4 can be of particular interest since internal light scattering in nanophosphors is negligible compared to bulk counterparts [3]. Also, nanophosphors show stronger luminescence emission compared to bulk ones due to the modification of radiative lifetimes [4].

So far no data on the radiative and nonradiative transition probabilities and quantum efficiencies of emission of RE impurities in Mg_2TiO_4 nanoparticles have been reported. These important emission characteristics are needed to compare luminescence performance of the RE ions in Mg_2TiO_4 with their performance in other, well established hosts. Therefore, we aimed in this work at an analysis of the Eu^{3+} ion emission in the Mg_2TiO_4 nanoparticles prepared with Pechini-type polymerized complex route [2, 5] at different, low temperatures. In addition to the experimental studies, the Judd-Ofelt analysis of the emission spectra of Eu^{3+} ions was performed, which allowed calculating radiative and nonradiative transition probabilities, Judd-Ofelt intensity parameters, and the quantum efficiency of the Eu^{3+} emission in the Mg_2TiO_4 nanoparticles. At low temperatures Mg_2TiO_4 structure is metastable; however, literature results indicate that crystallites of nanoscale dimensions may lead to a higher stability of some cubic phases [6, 7]. Therefore, the analysis should also provide the temperature that delivers Mg_2TiO_4 nanoparticles with best luminescence properties.

2. Experimental Part

2.1. Synthesis of Eu^{3+} Doped Mg_2TiO_4 Nanoparticles. Eu^{3+} doped Mg_2TiO_4 (2 at% of Eu) was synthesized with

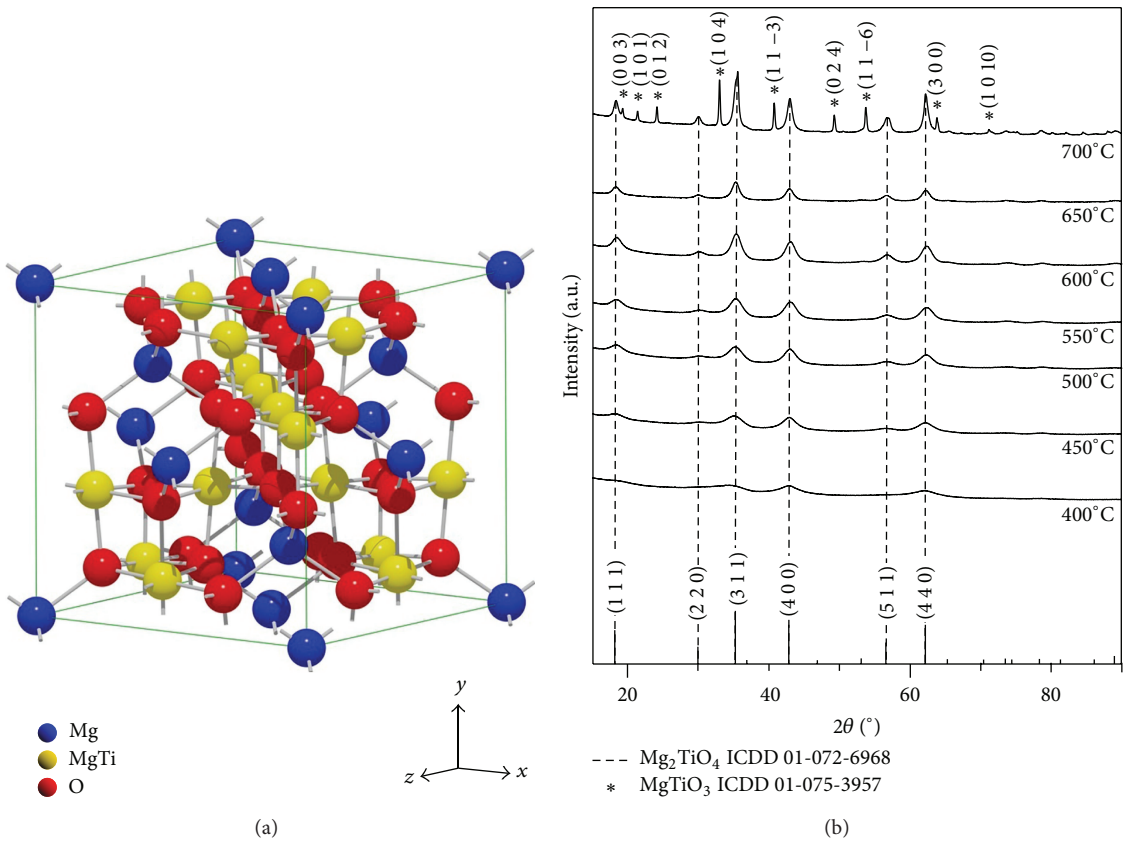

FIGURE 1: Crystal structure of Eu^{3+} activated Mg_2TiO_4: (a) schematic of the unit cell; (b) X-ray diffraction patterns of nanoparticles prepared at different temperatures from 400°C to 700°C.

Pechini-type polymerized complex route which is essentially based on the polyesterification between citric acid (CA) and ethylene glycol (EG) [2, 5]. Molar ratio of precursor components was magnesium oxide : titanium (IV)-isopropoxide : citric acid : ethylene glycol = 2 : 1 : 5 : 20. In the first step, titanium (IV)-isopropoxide (Alfa Aesar, 97%) was dissolved in ethylene glycol (Lach-Ner, 99%) under constant magnetic stirring at room temperature. Then, citric acid (Kemika, 99.5%) was added to the solution and stirred until complete dissolution was achieved. The appropriate amount of MgO and Eu_2O_3 were dissolved in concentrated nitric acid at 130°C, evaporated to dryness, and joined with titanium (IV)-isopropoxide/EG/CA mixture. In the next step, the mixture was stirred for 1 hour at 60°C until it becomes transparent and further stirred at 130°C for few hours. During this heating process, the formation of the polymer was promoted. As the colloidal solution was condensed and the excess of solvents removed, it became highly viscous, and this viscous polymeric product was decomposed at 350°C in 30 minutes to a dark mass precursor. This mass precursor was powdered and further calcined at 400°C, 450°C, 500°C, 550°C, 600°C, 650°C, and 700°C to obtain pure phase of Eu^{3+} doped Mg_2TiO_4 nanoparticles.

2.2. Instruments and Measurements. X-ray diffraction measurements were performed with Rigaku SmartLab diffractometer and data were recorded in a 2θ range from 15° to 120°, counting 0.7°/minute in 0.02° steps. Transmission electron microscopy was performed using JEOL-JEM 2100 LaB6 operated at 200 kV. Photoluminescence measurements were performed at room temperature on Fluorolog-3 Model FL3-221 spectrofluorometer system (Horiba Jobin-Yvon), utilizing 450W Xenon lamp as an excitation source for emission measurements and Xenon–Mercury pulsed lamp for lifetime measurements. The emission spectra were scanned in the range of wavelengths from 430 to 790 nm. The TBX-04-D PMT detector is used for both lifetime and steady state acquisitions. The line intensities and positions of the measured spectra were calibrated with a standard mercury-argon lamp.

3. Results and Discussion

3.1. Microstructural Analysis. Mg_2TiO_4 crystallize in a cubic, inverse spinel structure (Fd-3m space group) [8–10]. In this structure, Mg^{2+} ions are located in tetrahedral and octahedral sites while the Ti^{4+} ions occupy only octahedral sites, as shown in Figure 1(a). Arrangement of Ti^{4+} and Mg^{2+} ions in the octahedral sites is random.

X-ray diffraction patterns of samples calcined at different temperatures from 400°C to 700°C are presented in Figure 1(b). The main diffraction peaks are indexed according to ICDD01-072-6968 card. Pure phase of Mg_2TiO_4 is present in the samples annealed in the temperature range from 400°C

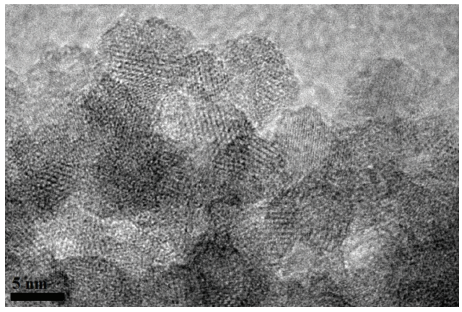

Figure 2: TEM image of the Eu^{3+} activated Mg_2TiO_4 nanoparticles prepared at 600°C.

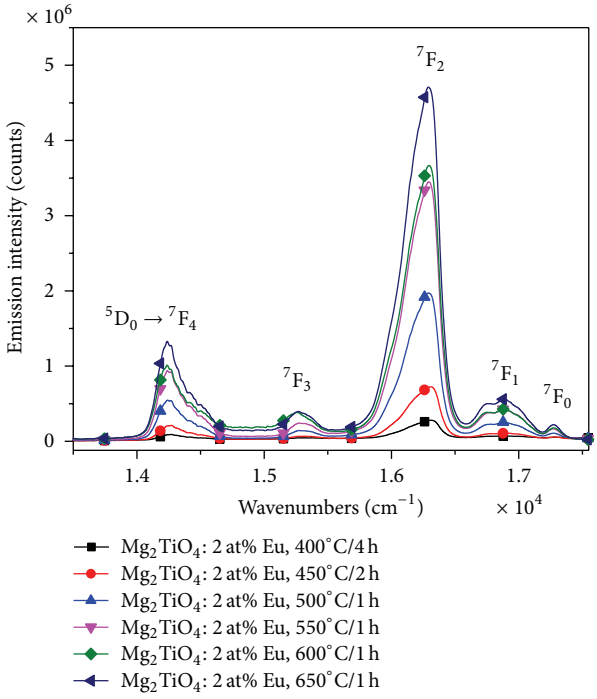

Figure 3: The emission spectra of the Eu^{3+} activated Mg_2TiO_4 nanoparticles prepared at different temperatures from 400°C to 650°C.

to 650°C. In the sample calcined at 700°C ilmenite ($MgTiO_3$) phase is presented along with Mg_2TiO_4.

TEM image in Figure 2 shows morphology of particles of Mg_2TiO_4 doped Eu^{3+} sample annealed at 600°C for 1 hour. The sample is composed of loosely agglomerated nanoparticles of 5 to 10 nm in diameter.

3.2. Photoluminescence Emission Spectra and Lifetime Measurements. The emission spectra of Mg_2TiO_4 samples doped with 2 at% Eu and annealed in the 400–650°C temperature range are presented in Figure 3. Due to even number of electrons in the 4f shell ($4f^6$ configuration), the crystal-field perturbation by the host matrix lifts partly or completely the degeneracies of the Eu^{3+} levels [11]. Therefore, emission spectra show five characteristic bands centered around 17271, 16892, 16287, 15290, and 14245 cm^{-1} that originate from $^5D_0 \rightarrow {}^7F_J$ ($J = 0, 1, 2, 3$, and 4) spin forbidden f-f electronic transitions of the Eu^{3+} ions. The $^5D_0 \rightarrow {}^7F_1$ transition is magnetic dipole in nature and follows the selection rule $\Delta J = 1$. Its intensity is independent of the host matrix. On the other hand, the $^5D_0 \rightarrow {}^7F_{2,4,6}$ are "the forced" (induced) electric dipole transitions, known to be forbidden by the Laporte selection rule and may occur due to the mixing of the 4f orbitals with opposite parity at the low symmetry sites. The $^5D_0 \rightarrow {}^7F_2$ is known as a hypersensitive transition because it is easily affected by the local environment around europium ion, and its intensity depends on the symmetry of crystal field around the europium ion. The intensity of $^5D_0 \rightarrow {}^7F_2$ transition is the most intense across the emission spectra. The $^5D_0 \rightarrow {}^7F_0$ transition is not allowed since 0–0 transitions are forbidden by the selection rule $J = 0 \rightarrow J' = 0$. The appearance of this transition is mainly due to the J-mixing effect [12] and indicates that Eu^{3+} ion is located in a site without an inversion center. Low energy transitions, $^5D_0 \rightarrow {}^7F_3$ and $^5D_0 \rightarrow {}^7F_4$, are also clearly visible. Emissions from $^5D_0 \rightarrow {}^7F_5$ (12990–13510 cm^{-1}) and $^5D_0 \rightarrow {}^7F_6$ (11900–12350 cm^{-1}) transitions could not be detected due to the instrument limitations.

Table 1: Lifetimes of the $^5D_0$ emission level of Eu^{3+} in Mg_2TiO_4 nanoparticles prepared at different temperatures.

Mg_2TiO_4 doped 2 at% Eu^{3+}	
Annealing temperature (°C)	Lifetime (μs)
400	573
450	741
500	818
550	853
600	872
650	851

From emission spectra (Figure 3) one can notice that the emission intensity increases with the increase of annealing temperature and that there is no significant change in the emission spectra's shape. The emission decays of the $^5D_0$ emitting level are obtained under 394 nm excitation. Average lifetime values are calculated using the following equation:

$$\tau_{\text{avg}} = \frac{\int_0^\infty tI(t)\,dt}{\int_0^\infty I(t)\,dt}, \quad (1)$$

where $I(t)$ represents the luminescence intensity (corrected for the background) at time t. The results are presented in Table 1.

In all samples the highest emission intensity is observed for $^5D_0 \rightarrow {}^7F_2$ transition. The intensity of this transition, Figure 2, and the lifetime values, Table 1, enlarge with the rise of the annealing temperature up to 650°C. These values, however, decrease in the sample prepared at 650°C.

3.3. Judd-Ofelt Calculations and Results. The Judd-Ofelt theory [13, 14] describes intensities of transitions of lanthanides

and actinides in solids and solutions, whereas Judd-Ofelt parameters characterize local structure and bonding in the vicinity of rare earth ions. This theory provides information about oscillator strengths, radiative lifetime, and emission probabilities. The analysis also provides values of quantum efficiency.

According to J-O theory [13, 14] theoretical expression for the oscillator strength of an induced electric dipole transition from the ground state to an excited state is

$$f = \frac{8\pi^2 mc\nu}{3h(2J+1)} \frac{\left(n^2+2\right)^2}{9n} \sum_{\lambda=2,4,6} \Omega_\lambda \left|\left\langle \Psi J \left\| U^{(\lambda)} \right\| \Psi J' \right\rangle\right|^2, \quad (2)$$

where h denotes Planck constant (6.626×10^{-34} J·s; 4.135×10^{-15} eV·s), $2J + 1$ is the degeneracy of the initial state, n is the refractive index, Ω_λ are the Judd-Ofelt parameters, and $\langle \Psi J \| U^{(\lambda)} \| \Psi J' \rangle$ terms are the double reduced matrix elements of unit tensor operators whose values are independent of the local environment of the ion. According to the Judd-Ofelt theory radiative transition probability, A, is related to its dipole strength according to the following equation:

$$A\left(\Psi' J'; \Psi' J'\right) = \frac{65\pi^4 e^2}{3h(2J'+1)\lambda^3} \left[n \left(\frac{n^2+2}{2} \right)^2 D_{\mathrm{ED}} + n^2 D_{\mathrm{MD}} \right], \quad (3)$$

where D_{ED} and D_{MD} represent the electric and magnetic dipole strengths, respectively. Transition probabilities of the rare earths are composed mainly of the electric dipole contribution $^5\mathrm{D}_0 \rightarrow {}^7\mathrm{F}_J$ ($J = 2, 4$) and to a much lesser extent by the magnetic-dipole contribution $^5\mathrm{D}_0 \rightarrow {}^7\mathrm{F}_1$. The $^5\mathrm{D}_0 \rightarrow {}^7\mathrm{F}_3$ transition is forbidden according to Judd-Ofelt theory, both in magnetic and induced electric dipole scheme, and this transition can only gain intensity via J-mixing [15, 16]. Also, the $^5\mathrm{D}_0 \rightarrow {}^7\mathrm{F}_0$ transition is strictly forbidden according to the standard Judd-Ofelt theory. Therefore, these two transitions will not be considered in determining transition probabilities. The intensity of $^5\mathrm{D}_0 \rightarrow {}^7\mathrm{F}_1$ magnetic dipole transition is largely independent of the environment and can be considered in a first approximation to be constant [17]. The magnetic dipole transition can be calculated by theory [15, 18]:

$$D_{\mathrm{MD}} = 9.6 \times 10^{-42}\ \mathrm{esu^2\,cm^2} = 0.96 \times 10^{-54}\ \mathrm{J \cdot m^3} = 5.99 \times 10^{-36}\ \mathrm{eV \cdot m^3}. \quad (4)$$

The strength of all induced electric dipole transitions is

$$D_{\mathrm{ED}}\left(J, J'\right) = e^2 \sum_{\lambda=2,4,6} \Omega_\lambda \left|\left\langle \Psi J \left\| U^{(\lambda)} \right\| \Psi J' \right\rangle\right|^2, \quad (5)$$

where squared reduced matrix elements $|\langle \Psi J \| U^{(\lambda)} \| \Psi J' \rangle|^2$ have values independent of the host matrix. For the case of Eu^{3+} these values are tabulated in [18–20], and Judd-Ofelt intensity parameters can be evaluated solely from the emission spectrum because nondiagonal elements of the $|\langle \Psi J \| U^{(\lambda)} \| \Psi J' \rangle|^2$ matrix have zero values according to the following equation:

$$\Omega_\lambda = \frac{D_{\mathrm{MD}} \nu_1^3}{e^2 \nu_\lambda^3} \frac{9n^3}{n\left(n^2+2\right)^2 \left|\left\langle \Psi J \left\| U^{(\lambda)} \right\| \Psi' J' \right\rangle\right|^2} \frac{\int I_\lambda(\nu_\lambda)}{\int I_1(\nu_1)}. \quad (6)$$

For the calculations, the value of refractive index of 1.691 for Mg_2TiO_4 is taken from the literature [21]. According to [22] radiative emission probability of magnetic dipole transition, $A\,(^5\mathrm{D}_0 \rightarrow {}^7\mathrm{F}_1)$, has value of 57.34 s^{-1} for the $50(NaPO_3)_6 + 10TeO_2 + 20AlF_3 + 19LiF + 1Eu_2O_3$ glass with a refractive index of 1.591. Taking this value as a reference, and with the well-known correction factor of $(n/1.591)^3$, which can be derived from the general equations for the magnetic dipole transition probability rates [23, 24], $A\,(^5\mathrm{D}_0 \rightarrow {}^7\mathrm{F}_1) = 68.85\ \mathrm{s}^{-1}$ is calculated for the radiative emission probability of magnetic dipole transition of Eu^{3+} in Mg_2TiO_4. The intensity of this transition can be considered as a reference for all transitions originating from the $^5\mathrm{D}_0$ excited state [11]. Then, it is possible to calculate radiative emission probabilities of all transitions originating from the $^5\mathrm{D}_0$ excited state from the ratios of areas S under corresponding emission bands in Figure 3 [20, 22]:

$$A\left(^5\mathrm{D}_0 \longrightarrow {}^7\mathrm{F}_{2,4}\right) = A\left(^5\mathrm{D}_0 \longrightarrow {}^7\mathrm{F}_1\right) \frac{S\left(^5\mathrm{D}_0 \longrightarrow {}^7\mathrm{F}_{2,4}\right)}{S\left(^5\mathrm{D}_0 \longrightarrow {}^7\mathrm{F}_1\right)}. \quad (7)$$

Total radiative emission probability, A_R, defined as the sum of all radiative emission probabilities:

$$A_R = \sum_{\lambda=1,2,4} A_\lambda, \quad (8)$$

can be further used to calculate nonradiative probability A_{NR} (which includes relaxation by multiphonon emission and effective energy transfer rates arising from ion-ion interactions [11]) and emission quantum efficiency η (the ratio between the number of photons emitted by the Eu^{3+} ion to the number of those absorbed):

$$A_{\mathrm{NR}} = \frac{1}{\tau} - A_{\mathrm{NR}}, \qquad \eta = \frac{A_R}{A_R + A_{\mathrm{NR}}}. \quad (9)$$

The Ω_2 intensity parameter describes hypersensitivity of $^5\mathrm{D}_0 \rightarrow {}^7\mathrm{F}_2$ transition since it is affected by the symmetry of local surrounding around the Eu^{3+} site. Ω_4 and Ω_6 parameters are associated with the viscosity and rigidity of the host material. Several reports [25–28] used Ω_2 to assess the magnitude of covalence between Eu^{3+} and surrounding ligands (the larger the Ω_2, the stronger the covalence); however one should note that there are number of competing

Table 2: Intensity parameters, radiative and nonradiative emission probabilities, quantum efficiencies, and asymmetry ratios of Eu^{3+} emission from Mg_2TiO_4 nanoparticles prepared at different temperatures from 400°C to 650°C.

T (°C)	Ω_2 (10^{-20} cm^{-2})	Ω_4 (10^{-20} cm^{-2})	A (s^{-1})	A_{NR} (s^{-1})	η (%)	R
400	5.23	2.94	309.68	1435.51	17.75	3.22
450	8.80	4.50	487.37	862.15	36.11	5.46
500	10.71	5.08	577.53	644.96	47.24	6.65
550	11.42	5.30	609.79	562.53	52.01	7.10
600	12.46	6.23	671.20	475.58	58.53	7.75
650	12.24	5.88	654.54	520.54	55.70	7.60

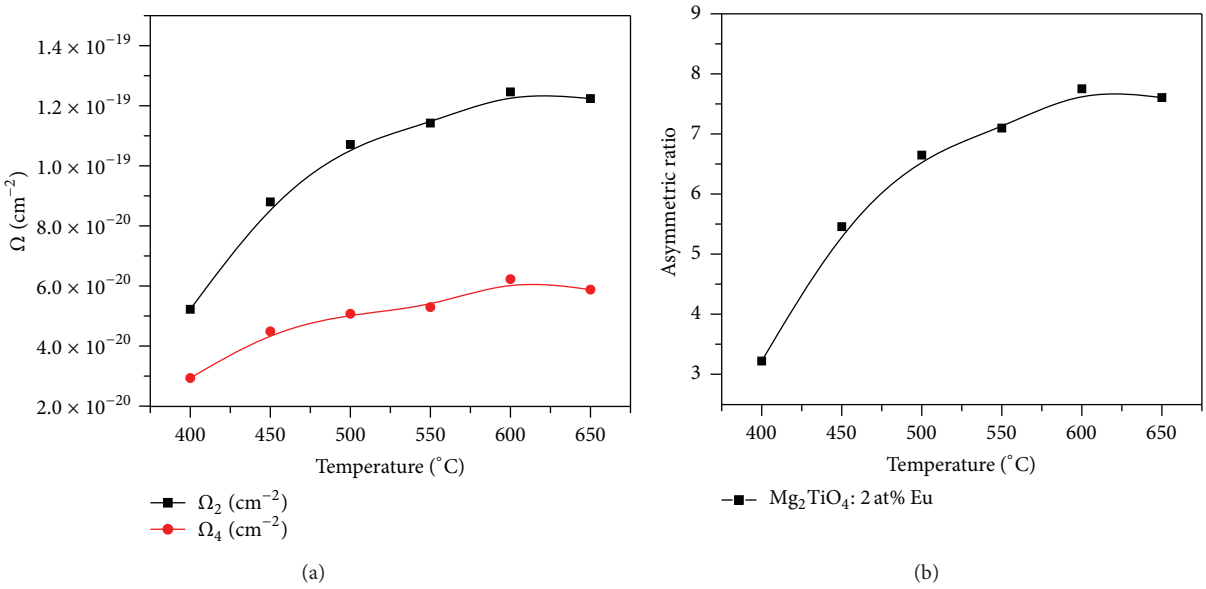

Figure 4: (a) Ω_2 (black squares) and Ω_4 (red circles) intensity parameters and (b) asymmetric ratio of Eu^{3+} emission in Mg_2TiO_4 nanoparticles prepared at different temperatures.

mechanisms for induced electric dipole transitions, so the dominant mechanism could not be determined from the single parameter. Luminescence intensity ratio $R = (^5D_0 \rightarrow {}^7F_2)/(^5D_0 \rightarrow {}^7F_1)$ is also known as asymmetry ratio [29]. Higher values of R indicate lower symmetry around the trivalent europium ions [30, 31]. Ω_2 and R reveal similar physical information on the bonding nature between Eu^{3+} ion and the surrounding anions and explain the short range effects in local structure around Eu^{3+} ions [28]. Ω_6 intensity parameter could not be determined because $^5D_0 \rightarrow {}^7F_6$ emission in this sample could not be detected due to the instrumental limitations.

Calculated Judd-Ofelt parameters show variation with the annealing temperature, and their values are presented in Table 2 along with the values of radiative and nonradiative emission probabilities, quantum efficiencies, and asymmetry ratios.

Ω_2 and Ω_4 dependence on temperature is displayed in Figure 4(a), and asymmetric ratio is presented in Figure 4(b). One can notice that the values of Ω_2 and Ω_4 increase with the increase of annealing temperature until 600°C. Eu^{3+} emission from the sample prepared at 650°C has lower values of Ω_2 and Ω_4 than in the case of sample prepared at 600°C. This result indicates that local environment of the Eu^{3+} ion changes at temperatures higher than 600°C. In the complete temperature range Ω_2 is larger than Ω_4. The relatively high value of Ω_2 and the observed trend indicate a relatively high asymmetry at the Eu^{3+} site. These results are in agreement with the values of luminescence intensity ratio: 3.23, 5.46, 6.65, 7.10, 7.75, and 7.60. One should notice the trend of R value increase with the annealing temperature up to 600°C and decrease for 650°C. A high value of this ratio indicates low symmetry of the crystal field around the europium ion due to distortion of the surrounding bonds [32]. The start of reverse trend of change of Judd-Ofelt parameters and asymmetric ratio at temperature of 650°C indicates the beginning of material structural disorder since at that temperature the decrease of quantum efficiency is also observed.

Figure 5(a) shows changes of radiative and nonradiative emission probabilities of Eu^{3+} emissions in samples prepared at different temperatures. Until 600°C radiative emission probability increases and nonradiative decreases. The trend reverses for sample prepared at 650°C. The quantum efficiency of emission, Figure 5(b), increases from 17.75% in sample annealed at 400°C to 58.53% for a sample prepared at 600°C. The quantum efficiency of Eu^{3+} emission in sample

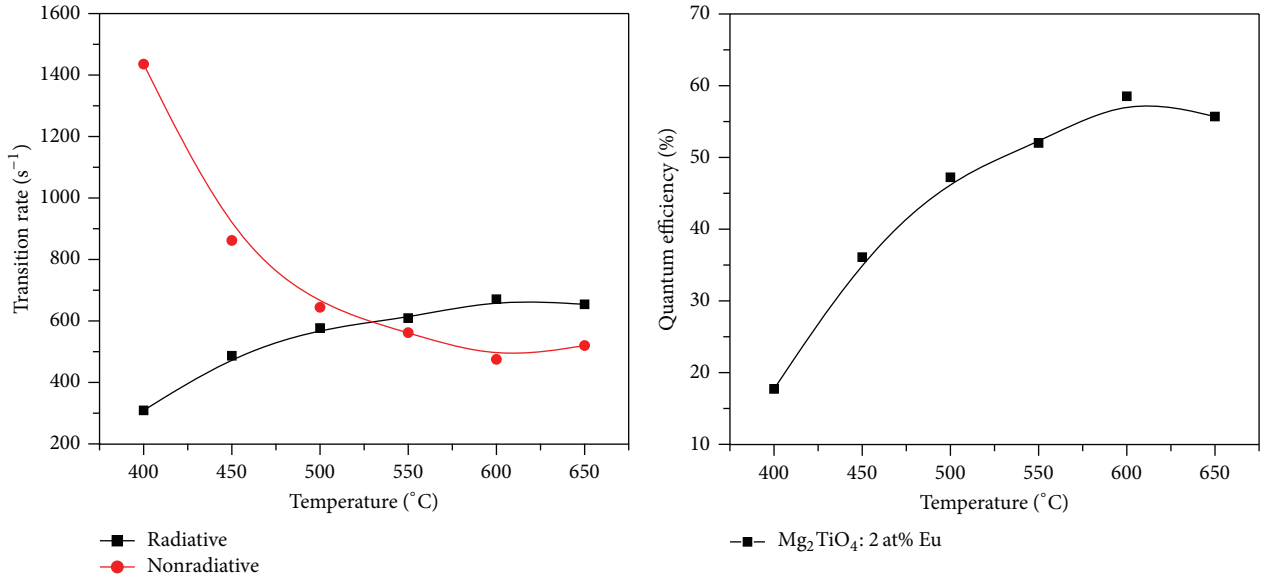

FIGURE 5: (a) Radiative (black squares) and nonradiative transition rates (red circles) and (b) quantum efficiency of Eu^{3+} emission in Mg_2TiO_4 nanoparticles prepared at different temperatures.

prepared at 650°C is 55.70%, lower than for sample prepared at 600°C.

One should note that the values of quantum efficiency are slightly underestimated, since calculation does not account $^5D_0 \rightarrow {}^7F_{3,5,6}$ emissions. However, the trend of quantum efficiency change with annealing temperature is unaffected by this deficiency. Also, refraction index is wavelength dependent physical property, so taking the constant value into calculation introduces error into results; however, the error is small since the refractive index changes are small over the wavelength region of interest [20]. These simplifications are justified for the sake of comparison of JO parameters and emission parameters between samples, since small errors cannot change observed trends. It is acknowledged that Judd-Ofelt theory estimates transition probabilities with accuracy generally not worse than 10% [33].

4. Conclusion

To conclude, Eu^{3+} doped Mg_2TiO_4 nanoparticles of about 5 to 10 nm in size can be prepared with Pechini-type polymerized complex route after annealing in the low-temperature range from 400°C to 650°C. The best luminescence properties showed nanoparticles prepared at 600°C exhibiting quantum efficiency of emission of 58.5% and emission lifetime of 872 μs. In all samples Judd-Ofelt intensity parameter Ω_2 was larger than Ω_4, and relatively high values of Ω_2 and asymmetry ratio are observed. The latter indicate relatively high asymmetry at the Eu^{3+} sites.

Conflict of Interests

The authors declare that there is no conflict of interests regarding the publication of this paper.

Acknowledgments

The authors acknowledge the financial support of the Ministry of Education and Science of the Republic of Serbia (Project no. 45020) and the support from the APV Provincial Secretariat for Science and Technological Development of the Republic of Serbia through Project no. 114-451-1850/2014-03.

References

[1] T. Ye, S. Li, X. Wu et al., "Sol-gel preparation of efficient red phosphor Mg_2TiO_4:Mn^{4+} and XAFS investigation on the substitution of Mn^{4+} for Ti^{4+}," *Journal of Materials Chemistry C*, vol. 1, no. 28, pp. 4327–4333, 2013.

[2] M. M. Medić, M. G. Brik, G. Dražić, Ž. M. Antić, V. M. Lojpur, and M. D. Dramićanin, "Deep-red emitting Mn^{4+} doped Mg_2TiO_4 nanoparticles," *Journal of Physical Chemistry C*, vol. 119, no. 1, pp. 724–730, 2014.

[3] G. Liu and X. Chen, "Spectroscopic properties of lanthanides in nanomaterials," in *Handbook on the Physics and Chemistry of Rare Earths*, J.-C. B. Karl, A. Gschneidner, and K. P. Vitalij, Eds., pp. 99–169, Elsevier, 2007.

[4] R. S. Meltzer, S. P. Feofilov, B. Tissue, and H. B. Yuan, "Dependence of fluorescence lifetimes of Y_2O_3:Eu^{3+} nanoparticles on the surrounding medium," *Physical Review B*, vol. 60, no. 20, pp. R14012–R14015, 1999.

[5] S. Ćulubrk, Ž. Antić, M. Marinović-Cincović, P. S. Ahrenkiel, and M. D. Dramićanin, "Synthesis and luminescent properties of rare earth (Sm^{3+} and Eu^{3+}) Doped $Gd_2Ti_2O_7$ pyrochlore nanopowders," *Optical Materials*, vol. 37, pp. 598–606, 2014.

[6] C. Huang, Z. Tang, Z. Zhang, and J. Gong, "Study on a new, environmentally benign method and its feasibility of preparing nanometer zirconia powder," *Materials Research Bulletin*, vol. 35, no. 9, pp. 1503–1508, 2000.

[7] P. R. Arya, P. Jha, and A. K. Ganguli, "Synthesis, characterization and dielectric properties of nanometer-sized barium strontium titanates prepared by the polymeric citrate precursor method," *Journal of Materials Chemistry*, vol. 13, no. 2, pp. 415–423, 2003.

[8] F. W. Barth Tom and E. Posnjak, "Spinel structures: with and without variate atom equipoints," *Zeitschrift für Kristallographie—Crystalline Materials*, vol. 82, no. 1, article 325, 1932.

[9] H. S. C. O'Neill, S. A. T. Redfern, S. Kesson, and S. Short, "An in situ neutron diffraction study of cation disordering in synthetic qandilite Mg_2TiO_4 at high temperatures," *American Mineralogist*, vol. 88, no. 5, pp. 860–865, 2003.

[10] R. L. Millard, R. C. Peterson, and B. K. Hunter, "Study of the cubic to tetragonal transition in Mg_2TiO_4 and Zn_2TiO_4 spinels by 17O MAS NMR and rietveld refinement of X-ray diffraction data," *American Mineralogist*, vol. 80, no. 9-10, pp. 885–896, 1995.

[11] K. Binnemans, "Interpretation of europium(III) spectra," *Coordination Chemistry Reviews*, vol. 295, pp. 1–45, 2015.

[12] P. A. Tanner, Y. Y. Yeung, and L. Ning, "What factors affect the $^5D_0$ energy of Eu^{3+}? An investigation of nephelauxetic effects," *The Journal of Physical Chemistry A*, vol. 117, no. 13, pp. 2771–2781, 2013.

[13] B. R. Judd, "Optical absorption intensities of rare-earth ions," *Physical Review*, vol. 127, no. 3, pp. 750–761, 1962.

[14] G. S. Ofelt, "Intensities of crystal spectra of rare−earth ions," *The Journal of Chemical Physics*, vol. 37, no. 3, pp. 511–520, 1962.

[15] M. J. Weber, T. E. Varitimos, and B. H. Matsinger, "Optical intensities of rare-earth ions in yttrium orthoaluminate," *Physical Review B*, vol. 8, no. 1, pp. 47–53, 1973.

[16] J. E. Lowther, "Spectroscopic transition probabilities of rare earth ions," *Journal of Physics C: Solid State Physics*, vol. 7, no. 23, pp. 4393–4402, 1974.

[17] C. Görller-Walrand, L. Fluyt, A. Ceulemans, and W. T. Carnall, "Magnetic dipole transitions as standards for Judd-Ofelt parametrization in lanthanide spectra," *The Journal of Chemical Physics*, vol. 95, no. 5, pp. 3099–3106, 1991.

[18] M. H. V. Werts, R. T. F. Jukes, and J. W. Verhoeven, "The emission spectrum and the radiative lifetime of Eu^{3+} in luminescent lanthanide complexes," *Physical Chemistry Chemical Physics*, vol. 4, no. 9, pp. 1542–1548, 2002.

[19] W. T. Carnall, P. R. Fields, and K. Rajnak, "Spectral intensities of the trivalent lanthanides and actinides in solution. II. Pm^{3+}, Sm^{3+}, Eu^{3+}, Gd^{3+}, Tb^{3+}, Dy^{3+}, and Ho^{3+}," *The Journal of Chemical Physics*, vol. 49, no. 10, pp. 4412–4423, 1968.

[20] L. Dačanin, S. R. Lukić, D. M. Petrović, M. Nikolić, and M. D. Dramićanin, "Judd-Ofelt analysis of luminescence emission from Zn_2SiO_4:Eu^{3+} nanoparticles obtained by a polymer-assisted solgel method," *Physica B: Condensed Matter*, vol. 406, no. 11, pp. 2319–2322, 2011.

[21] M. J. Weber, *Handbook of Optical Materials*, CRC Press, Boca Raton, Fla, USA, 2003.

[22] D. Uma Maheswari, J. Suresh Kumar, L. R. Moorthy, K. Jang, and M. Jayasimhadri, "Emission properties of Eu^{3+} ions in alkali tellurofluorophosphate glasses," *Physica B: Condensed Matter*, vol. 403, no. 10-11, pp. 1690–1694, 2008.

[23] J. C. Boyer, F. Vetrone, J. A. Capobianco, A. Speghini, and M. Bettinelli, "Variation of fluorescence lifetimes and judd-ofelt parameters between Eu^{3+} doped bulk and nanocrystalline cubic Lu_2O_3," *Journal of Physical Chemistry B*, vol. 108, no. 52, pp. 20137–20143, 2004.

[24] C. Liu, J. Liu, and K. Dou, "Judd-Ofelt intensity parameters and spectral properties of Gd_2O_3:Eu^{3+} nanocrystals," *Journal of Physical Chemistry B*, vol. 110, no. 41, pp. 20277–20281, 2006.

[25] C. Koeppen, S. Yamada, G. Jiang, A. F. Garito, and L. R. Dalton, "Rare-earth organic complexes for amplification in polymer optical fibers and waveguides," *Journal of the Optical Society of America B: Optical Physics*, vol. 14, no. 1, pp. 155–162, 1997.

[26] S. S. Braga, R. A. Sá Ferreira, I. S. Gonçalves et al., "Synthesis, characterization, and luminescence of β-cyclodextrin inclusion compounds containing europium(III) and gadolinium(III) tris(β-diketonates)," *The Journal of Physical Chemistry B*, vol. 106, no. 44, pp. 11430–11437, 2002.

[27] G. Ehrhart, M. Bouazaoui, B. Capoen et al., "Effects of rare-earth concentration and heat-treatment on the structural and luminescence properties of europium-doped zirconia sol-gel planar waveguides," *Optical Materials*, vol. 29, no. 12, pp. 1723–1730, 2007.

[28] P. Babu and C. K. Jayasankar, "Optical spectroscopy of Eu^{3+} ions in lithium borate and lithium fluoroborate glasses," *Physica B: Condensed Matter*, vol. 279, no. 4, pp. 262–281, 2000.

[29] A. Patra, E. Sominska, S. Ramesh et al., "Sonochemical preparation and characterization of Eu_2O_3 and Tb_2O_3 doped in and coated on silica and alumina nanoparticles," *The Journal of Physical Chemistry B*, vol. 103, no. 17, pp. 3361–3365, 1999.

[30] K. Binnemans, K. Van Herck, and C. Görller-Walrand, "Influence of dipicolinate ligands on the spectroscopic properties of europium(III) in solution," *Chemical Physics Letters*, vol. 266, no. 3-4, pp. 297–302, 1997.

[31] M. Kumar, T. K. Seshagiri, and S. V. Godbole, "Fluorescence lifetime and Judd–Ofelt parameters of Eu^{3+} doped $SrBPO_5$," *Physica B: Condensed Matter*, vol. 410, no. 1, pp. 141–146, 2013.

[32] V. Đorđević, Ž. Antić, M. G. Nikolić, and M. D. Dramićanin, "Comparative structural and photoluminescent study of Eu^{3+}-doped La_2O_3 and $La(OH)_3$ nanocrystalline powders," *Journal of Physics and Chemistry of Solids*, vol. 75, no. 2, pp. 276–282, 2014.

[33] R. Rolli, K. Gatterer, M. Wachtier, M. Bettinelli, A. Speghini, and D. Ajò, "Optical spectroscopy of lanthanide ions in ZnO-TeO_2 glasses," *Spectrochimica Acta Part A: Molecular and Biomolecular Spectroscopy*, vol. 57, no. 10, pp. 2009–2017, 2001.